Warping and Cracking of the Pacific Plate by Thermal Contraction

David Sandwell & Yuri Fialko

Scripps Institution of Oceanography, La Jolla, California, 92093-0225, USA

Submitted to Journal of Geophysical Research, March 16, 2004.

Lineaments in the gravity field and associated chains of volcanic ridges are widespread on the Pacific plate but are not yet explained by plate tectonics. We propose that they are warps and cracks in the plate caused by uneven thermal contraction of the cooling lithosphere. Top-down cooling of the plate produces large thermoelastic stress that is optimally released by lithospheric flexure between regularly spaced parallel cracks. Both the crack spacing and gravity amplitude are predicted by elastic plate theory and variational principle. Cracks along the troughs of the gravity lineaments provide conduits for the generation of volcanic ridges in agreement with new observations from satellite-derived gravity. Our model suggests that gravity lineaments are a natural consequence of lithospheric cooling so that convective rolls or mantle plumes are not required.

Introduction

Plate tectonics explains most of the topography of the deep ocean basins, but there is still debate regarding the origin of off-ridge features that are younger than the ambient lithosphere, and especially those that are not aligned with the autochtonic seafloor spreading fabric. The Pacific basin contains three main types of the young off-ridge lineaments (Figure 1). (i) Chains of shield volcanoes such as the Hawaiian-Emperor seamounts are well explained by the mantle plume model [*Morgan*, 1971; *Sleep*, 1992]. (ii) Gravity lineaments are prominent at 140-200 km wavelength and are aligned in the direction of absolute plate motion [*Haxby and Wessel,* 1986] (Figure 1b). (iii) En-echelon volcanic ridges appear to be related to the gravity lineaments and have morphology consistent with the ridge-parallel extensional stress [*Winterer and Sandwell*, 1987; *Sandwell et al.*, 1995; *Lynch*, 1999] (Figure 2). The origin of both the gravity lineaments and the linear volcanic ridges has been the subject of many studies and field experiments [*Haxby and Weissel*, 1986; *Dunbar and Sandwell*, 1988; *Fleitout et al.*, 1989; *Forsyth et al.*, 2002; *Gans et al.*, 2003].

Several mechanisms have been proposed to explain the gravity lineaments (Figure 3), including small-scale convective rolls [*Haxby and Weissel*, 1986]; mini-hotspots [*Fleitout et al.*, 1989]; and extension of the lithosphere or boudinage [*Dunbar and Sandwell*, 1988]. Radiometric ages of the Pukapuka ridges in the Central Pacific are inconsistent with the mini hotspot model [*Sandwell et al.*, 1995]. The morphology of these volcanic ridges indicates that magma is extruded along cracks that are parallel to the absolute plate motion direction. Also, the chemistry of the dredged basalts is inconsistent with deep melting of plume material [*Janney et al.*, 2000]. The small-scale

convection model predicts extension and volcanism on the crests of the gravity lineaments (Figure 3) but qualitative observation show that the volcanic ridges preferentially occur in the troughs [*Winterer and Sandwell*, 1987; *Searle et al.*, 1995; *Sandwell et al.*, 1995; *Forsyth et al.*, 2002]. The boudinage model correctly predicts the characteristic wavelength of the gravity lineaments and the location of the volcanic ridges but at least 10% extension is needed to explain their observed amplitude [*Dunbar and Sandwell*, 1988]. Plate tectonic measurements of fracture zone spacing show that this amount of relative extension did not occur [*Goodwillie and Parsons*, 1992] and a recent study limits the extension to less than 2% [*Gans et al.*, 2003]. Thus the alternative explanations are certainly warranted. Here we provide new observational evidence and theoretical arguments indicating that both the gravity lineaments and volcanic ridges result from cooling and thermal contraction of the oceanic lithosphere, and are a natural consequence of plate tectonics.

Cooling and shrinkage of the oceanic lithosphere is a well-understood phenomenon that is responsible for the increase in seafloor depth with age [*Parsons and Sclater*, 1977]. Non-uniform shrinkage of the plate, mostly driven by the temperature gradients in the top part of the lithosphere, will result in the development of thermoelastic stresses that are large enough to fracture the plate [*Turcotte*, 1974; *Bratt et al.*, 1985; *Parmentier and Haxby*, 1986; *Sandwell*, 1986; *Wessel*, 1992]. Because the thickness of the lithosphere is small compared to its horizontal dimensions, and the seafloor is a stress-free boundary, the vertical component of the deviatoric stress is small and can be neglected. Under the thin plate approximation, the horizontal components of thermo-elastic stress can be decomposed into a thermal end load and a thermal bending moment [*Boley and Weiner*, 1960]. The thermal end loads can be partially relieved by plate-wide shrinkage, especially near the magmatically robust ridge axis which is unable to support large deviatoric stresses [*Parsons and Thompson*, 1991; *Fialko*, 2001]. However, even a plate with free ends may experience large thermoelastic stress, with compressional stress near the surface and tensional stress at depth [*Parmentier and Haxby*, 1986; *Wessel*, 1992]. The same physics describes tempering of glass sheets, whereby the residual compression at the surface inhibits the development of tensile fractures [*Woo*, 1968]. The predicted pattern of thermoelastic deformation is consistent with the focal mechanisms of intraplate earthquakes [*Weins and Stein*, 1984; *Bergman and Solomon*, 1984; *Shen et al.*, 1997]. Recently, *Gans et al*. [2003] proposed that the gravity lineaments are caused by convex upward flexure of the plate between regularly spaced lithospheric cracks where the flexure is driven by thermoelastic bending moment. While their model shows fair agreement with the observations, it does not explain why cracks develop with a particular spacing; they assume a 150-km spacing to match the observed spacing.

Here we refine and test the thermal contraction model to explain the origin of both the volcanic ridges and the gravity lineaments through a quantitative analysis of gravity data, as well as by developing a numerical model of thermoelastic flexure. We address the following questions. i) How do the gravity lineaments develop in amplitude and wavelength as a function of seafloor age? ii) Does the intraplate volcanism indeed preferentially occur in the troughs of the gravity lineaments? These first two questions are addressed using the gravity anomalies derived from reprocessing of the raw radar waveforms of ERS-1 satellite altimeter data. iii) Is there sufficient thermal bending moment to explain the amplitudes of both the gravity lineaments and the associated topography? iv) Finally, what mechanism controls the regular spacing of cracks of the

order of the flexural wavelength? One of the most important aspects of the thermoelastic model is that both the amplitude and spacing of the gravity lineaments are predicted from quantifying a process that is fundamental to plate tectonics, namely, the thermal contraction of the oceanic lithosphere.

Gravity lineaments and volcanic ridges from satellite altimetry

The central Pacific gravity lineaments were first discovered from the analysis of Seasat altimeter data [*Haxby and Weissel*, 1986]. While the track spacing and resolution of the Seasat data was sufficient to reveal the 140-200 km gravity lineaments, the discovery of volcanic ridges required better coverage and higher precision. The ERS-1 satellite altimeter increased the coverage during its geodetic phase (1994-95) and the higher quality Geosat altimeter data were declassified in 1995 [*Sandwell and Smith*, 1997]. Since the volcanic ridges are typically only 20 km wide and usually less than 1000 m tall, most were not visible above the 5-7 mGal noise level in the altimeter-derived gravity anomaly maps. Guided by these noisy gravity maps, several sets of ridges were surveyed by multibeam sonar (Figure 1a, shaded areas): Crossgrain ridges [*Winterer and Sandwell*, 1987]; Pukapuka ridges [*Sandwell et al.*, 1995]; the ridges of *Searle et al.* [1995]; and most recently the Sojourn Ridges [*Forsyth et al.*, 2002]. These sets of ridges appear to be preferentially located in the troughs of the gravity lineaments although there has been no quantitative confirmation of this observation.

To confirm the spatial correlation between the ridges and the gravity lineaments, we improve the resolution of the ERS-1 altimeter data by re-tracking the raw altimeter waveforms [*Maus et al.*, 1998] (Figure 1a). The retracking increases the short-wavelength precision by nearly a factor of 2, so the quality of the ERS-1 data is now superior to the Geosat data (not re-tracked yet). A new gravity model was constructed using all available altimeter profiles (see version 11 at http://topex.ucsd.edu). The rms deviation between two shipboard profiles and the new gravity model is 3.2 mGals in this area (Figure 4).

The gravity field of the small-scale ridges was separated from the larger scale lineaments using isotropic filters (Figure 1b). First, a low-pass filter was used to isolate features with wavelength shorter than about 80 km. This consisted of a median filter with a full-width of 65 km followed by a low-pass filter with a cosine taper between wavelengths of 108 and 54 km. The total gravity field minus this low-pass filtered gravity was clipped at 10 mGal to identify volcanic features (black areas in Figures 1bcd) in excellent agreement with multibeam surveys [*Lynch,* 1999; *Forsyth et al.*, 2002]. To isolate the gravity lineaments, the low-pass filtered part of the gravity field was further high-pass filtered for wavelengths greater than 600 km. Note that isotropic filters were used yet the residual fields are highly anisotropic; both the gravity lineaments and ridges are oriented in approximately the direction of the absolute motion of the Pacific plate over the Hawaiian hotspot (Figure 1b).

Profiles of band-pass filtered gravity reveal the development of the gravity lineaments on young seafloor (Figure 5). The profile closest to the East pacific Rise (EPR) has very low amplitude and little, if any, periodic variations in the gravity field. The profile to the west (3.2 Ma) reveals partially developed gravity lineaments (5 mGal peak-to-trough amplitude and 120 km wavelength). The amplitude and wavelength of the gravity lineaments increases with increasing seafloor age; by 8.2 Ma they are fully developed (10 mGal amplitude and 160-km wavelength). There is an indication that the wavelength increases to about 200 km on older seafloor. The gravity lineaments cut

across the grain of the older seafloor (> 20 Ma) indicating they are younger than the ambient lithosphere.

A visual examination of the area of most intense gravity lineaments suggests that the volcanic ridges are preferentially located in the troughs (Figure 1b – test area). Here we provide quantitative measures of this observation. First consider that the expected gravity field above the crest of a volcanic ridge will have two contributions – one from the ridge and a second from its flexural compensation. No matter how these data are band-pass filtered, the gravity should always be positive at the ridge axis since the gravity-to-topography ratio is positive at all wavelengths for all flexural compensation models. To further confirm this statement, we performed a simulation of flexural loading of a 5-km thick elastic plate [*Goodwillie and Watts*, 1993] using our identified distribution of volcanic ridges in the test area. In the absence of gravity lineations, the model predicts a 1.57 mGal shift in the ridge-sampled, band-pass filtered gravity.

We use two approaches to show that the volcanic ridges in the test area (Figure 1) are not randomly dispersed with respect to the gravity lineaments. First we sample the band-pass filtered gravity at all every location and median-filter the data over a 450-km diameter area. As expected the mean and median of the band-pass filtered gravity is close to zero everywhere (Figure 1c). However, if we sample only at the locations of the volcanic features, distinct patterns emerge (Figure 1d). Areas of large volcanoes, west of –135˚ longitude, preferentially sample highly-positive, band-pass filtered gravity as expected. Smaller volcanoes (~1000 m tall) sample moderately-positive, band-pass filtered gravity except in the areas of intense gravity lineations where they preferentially sample the valleys of the gravity rolls (blue in Figure 1d).

To further quantify this analysis, we examine the statistics of these samples (Figure 6). Volcanic ridges in the control area (Figure 1b) have mean value 1.39 mGal in agreement with the simulation above (median=0.70 mGal, standard deviation=4.10 mGal). However, in the test area we find the mean and median of the histogram is shifted to negative values (mean = -0.98 mGal, median= -0.73, standard deviation = 3.88 mGal). The difference between mean of the test area and the mean of the control area is –2.37 mGal . With 386 degrees of freedom corresponding to the independent volcanoes in the test area, the expected uncertainty in the mean is 0.197 mGal so the shift of –2.37 cannot due to random variations. This demonstrates that the volcanic ridges are indeed preferentially located in the troughs of the gravity lineaments. The small-scale convection model (Figure 3b) cannot be reconciled with these observations (in particular, by assuming that the gravity lows are caused by subsidence due to volcanic loading).

Thermoelastic cracking of the lithosphere

Turcotte [1974] proposed that thermal stresses caused by cooling of the lithosphere may be responsible for transform faults which act to relieve the stress. He provided an analytic solution for the plate flexure that will develop when the plate is subjected to bending moments at its edges. More recent studies [*Parmentier and Haxby*, 1986; *Wessel*, 1992] have noted that if the plate is free to contract while it is cooling, a downward bending moment will increase almost linearly with the age of the plate. The upper third of the plate will be in compression while the lower two thirds will be in tension. These calculations consider the finite yield strength of the lithosphere which becomes especially important in limiting the near surface stress. *Gans et al.* [2003] use these estimates of increasing thermal bending moment and

Turcotte's analytic flexure solution to explain the amplitude of the gravity lineaments in the Pacific plate. For a crack spacing of 150 km their calculations shows the development of 100 m of peak-to-trough plate flexure at an age of 3 Ma. However, their model does not explain the observed crack spacing and it also underestimates the amplitudes of the gravity lineaments. Here we present a theoretical model of yielding of the thermoelasically-deformed lithosphere that is based on the variational principle. In particular, we postulate that the lithosphere will deform in a way that will minimize the overall mechanical energy stored in a plate. We search for the crack spacing that liberates the maximum mechanical energy, and show that the optimal crack spacing is of the order of the flexural wavelength.

Consider a plate of length L with ends subjected to a bending moment M_T due to accumulation of thermoelastic stress. *Turcotte* [1974] provides an analytic solution for the deflection of a thin elastic plate floating on a fluid half space of density ρ (3300 kg m^{-3}). The plate deflection w, and curvature w'', are

$$w(x) = A\cos\frac{x}{\alpha}\cosh\frac{x}{\alpha} + B\sin\frac{x}{\alpha}\sinh\frac{x}{\alpha} \tag{1}$$

$$w''(x) = \frac{-2A}{\alpha^2}\sin\frac{x}{\alpha}\sinh\frac{x}{\alpha} + \frac{2B}{\alpha^2}\cos\frac{x}{\alpha}\cosh\frac{x}{\alpha}$$

where $\alpha = \left(\frac{4D}{\Delta\rho g}\right)^{1/4}$ is the flexural parameter, $D = \frac{EH^3}{12\left(1-\nu^2\right)}$ is the flexural rigidity, E is the Young's modulus (65 GPa), H is the plate thickness, ν is the Poisson's ratio (0.25), $\Delta\rho$ is the density difference between mantle and seawater, and g is the acceleration of gravity (9.8 m s^{-2}). The coefficients A and B are given by

$$A = \frac{\cos\theta\sinh\theta - \sin\theta\cosh\theta}{\sin\theta\cos\theta + \sinh\theta\cosh\theta}\frac{M_T\alpha^2}{2D} \tag{2}$$

$$B = \frac{\cos\theta\sinh\theta + \sin\theta\cosh\theta}{\sin\theta\cos\theta + \sinh\theta\cosh\theta}\frac{M_T\alpha^2}{2D}$$

where $\theta = \frac{L}{2\alpha}$.

Energy released by flexure

To predict the optimal crack spacing we calculate the energy released by the flexure. The change in the potential energy of elastic deformation stored in a plate is $F = \int_V \sigma(\mathbf{x})\varepsilon(\mathbf{x})dV$ where σ is the stress perturbation, and ε is the strain perturbation about some reference (e.g., lithostatic) state of deformation, and the integration is performed over the entire plate volume V. Prior to the onset of flexure, the stress σ equals the thermoelastic stress $\sigma_T(z)$ induced by the plate cooling, and the strain ε is

zero. After cracking, individual segments of the plate will experience elastic flexure such that the change in stress and strain components may be written as

$$\begin{array}{ll} \underline{\text{initial}} & \underline{\text{final}} \\ \varepsilon(z) = 0 & \varepsilon(z) \\ \sigma(z) = \sigma_T(z) & \sigma(z) = \sigma_T(z) + \dfrac{E}{\left(1-\nu^2\right)}\varepsilon(z) \end{array} \qquad (3)$$

For a quasi-static deformation, the change in energy Δf from the initial state to the final state is independent of path and equals

$$\Delta f = \frac{E\left(\Delta\varepsilon\right)^2}{\left(1-\nu^2\right)} + \sigma_T \Delta\varepsilon \qquad (4)$$

The first term in (4) is the energy needed (consumed) to flex the plate while the second term is the thermo-elastic energy released. Now consider the net energy released when equally spaced cracks are introduced in a cooled plate containing thermoelastic prestress σ_T (Figure 7). The plate has length S and width W and contains N longitudinal cracks with spacing L. The total elastic energy released, normalized by the area of the plate, is the energy density Q and it is given by

$$Q = \frac{F}{SW} = \frac{1}{SW}\iiint_V \sigma(\mathbf{x})\varepsilon(\mathbf{x})\,dzdxdy \qquad (5).$$

Noting that the problem is plane strain (there is no deformation along the y-axis), and $L=W/N$, one can re-write the energy density as

$$Q = \frac{1}{L}\int_{-L/2}^{L/2}\int_{-H/2}^{H/2}\sigma(x,z)\varepsilon(x,z)\,dzdx \qquad (6)$$

We expand the integrand in (6) using the expressions for energy change (4). For a thin plate flexure, $\varepsilon(z) = -zw''$ where z is the distance from the center of the plate and w'' is the plate curvature given in (1). The integral (6) becomes

$$Q = \frac{1}{L}\left\{\int_{-L/2}^{L/2}\left[w''(x)\right]^2\int_{-H/2}^{H/2}\frac{E}{\left(1-\nu^2\right)}z^2\,dzdx - \int_{-L/2}^{L/2}w''(x)\int_{-H/2}^{H/2}\sigma_T(z)z\,dzdx\right\} \qquad (7)$$

The first term on the right-hand side of equation (7) is the energy consumed by flexure of the plate. The second term is the thermoelastic energy released during the flexure. Note that the integral over z in the first term is the flexural rigidity D while the integral over z in the second term is the thermal bending moment M_T. Thus expression (7) can be written as

$$Q = \frac{D}{L}\int_{-L/2}^{L/2}\left[w''(x)\right]^2 dx - \frac{M_T}{L}\int_{-L/2}^{L/2}w''(x)\,dx \qquad (8)$$

For both terms, the energy depends on the curvature of the plate, but note that the energy consumed by plate flexure is always positive since it depends on the curvature squared while the thermoelastic energy released by flexure depends on the sign of the curvature. Concave downward flexure releases thermoelastic energy. By differentiating the expression (7) with respect to the crack spacing L, we find that Q has a global minimum at $L_c \approx 3.389\alpha$ (Figure 8), corresponding to the maximum energy release.

It is reasonable to assume that in the presence of random variations in the lithospheric strength and initial yielding induced by thermoelastic stresses, the subsequent deformation will be eventually localized on the optimally spaced macroscopic fracture zones. The occurrence of volcanic ridges along the presumed trans-lithospheric cracks suggests that the crack formation is caused (or assisted by) the magma fracture, whereby the ascending dikes relieve the deviatoric stress in the lithosphere. This mechanism implies that the crack zone is "weak" only during the dike emplacement; after the stress is re-set and the magmatic activity ceases, the mechanical properties of a "cracked" plate do not differ substantially from those of an "intact" plate. Alternatively, the thermoelastic stresses might be relieved primarily by thrust and normal faulting in the shallow and deep sections of the plate, respectively. Even in this case the subsequent magma intrusions are likely to substantially reduce the deviatoric stresses in the lithosphere along the crack zones, as dikes won't be able to deliver magma to the surface due to the negative dike buoyancy under the normal faulting conditions, and the unfavorable magma fracture orientation under the thrust faulting conditions. The dike intrusions will first relax the extensional stresses at the bottom of the plate, transferring the extension to shallower levels, and allowing the sub-vertical magma transport in the upper section of the plate. Regardless of whether the lithospheric crack zones are "hot" (magma-induced) or "cool" (amagmatic), the crack spacing predicted by our model is controlled only by the flexural wavelength of the lithosphere, and is in excellent agreement with observations (Figure 5). Note that the volcanic activity associated with the inferred crack zones implies the presence of partial melt in the sub-lithospheric mantle. This melt may represent remnant magma not extracted from the mantle at the ridge axis, or re-heating of the asthenosphere by plumes of the Superswell area [*Janney et al.*, 2000]. The orientation of cracks induced by the thermoelastic deformation is controlled by intraplate stresses. In particular, the cracks are predicted to align perpendicular to the least compressive stress.

Amplitude and wavelength of gravity lineaments

We use the method of *Wessel* [1992] to incrementally compute the evolution of thermo-elastic stress versus depth. At each time step we allow the end load to relax to zero and then check that the stress does not exceed the yield strength envelope [*Goetze and Evans*, 1979]. Our estimates of thermoelastic bending moment are 1.6 times greater than the estimates given in *Gans et al.,* [2003] but are in agreement with Wessel's calculations. The results of these calculations are shown in Figure 9 where we allow thermoelastic bending moment M_T to develop for some period of time before the cracks with spacing L are introduced (the onset time). The flexural rigidity D at the onset time is computed using the portion of the plate where the yield strength exceeds 20 MPa which roughly corresponds to the depth to the 600˚C isotherm. The corresponding values of D and M_T are then used in equation (1) to calculate the flexural topography. For this case of 130-km crack spacing, and 6 Ma onset time the peak-to-trough flexural

amplitude is about 200 m and the filtered gravity amplitude is 5 mGal (Figure 9a). We also calculate the flexural energy consumed and the thermoelastic energy released as a function of distance perpendicular to the cracks for an onset time of 6 Ma (Figure 9b). The net energy released is zero near the ends of the flexure. This illustrates why the model discourages the small crack spacing as being unable to efficiently relieve the thermoelastic stress (although the thin plate approximation obviously becomes inapplicable when the crack spacing L is not large compared to the plate thickness H). Towards the center of the flexure the thermoelastic energy released is greater than the flexural energy consumed because the thermal pre-stress exceeds the flexural stress. Note that if the curvature of the plate becomes concave upward, the pre-stress must increase in magnitude resulting in energy consumption. Therefore there is also an energy penalty when the crack spacing exceeds the critical wavelength L_c.

Because the flexural parameter scales with the plate thickness, $\alpha \propto H^{3/4}$, the optimal crack spacing increases with the increasing age of the lithosphere (Figure 9c). So far we have assumed that the fracture energy required for the crack formation is negligible compared to the energy balance (8). Our dimensional estimates of the thermoelastic energy release seem to justify this assumption (Figure 9c). Although the in situ fracture energy E_F is not well known, and may be scale-dependent, we use values derived from the laboratory measurements (10^2-10^3 Jm^{-2} for the tensile fracture energy [*Atkinson*, 1987; *Fialko and Rubin*, 1997]) and earthquake data (10^4-10^7 Jm^{-2} for the shear fracture energy [*Husseini*, 1977; *Scholz*, 2002]) to place an upper bound on work spent on inelastic deformation. For the problem shown in Figure 3c, the work spent on creating the cracks per unit area of the seafloor is $E_F H/L$. Thus the fracture energy enhances a penalty for the small crack spacing. Assuming E_F=10^7 Jm^{-2} , H=15 km, and L=150 km, we obtain $E_F H/L \sim O(10^6)$ Jm^{-2}, i.e., small compared to the thermoelastic energy density for the lithosphere older than 1-2 Ma (10^7-10^8 Jm^{-2}, Figure 9c). However, the fracture energy might not be negligible in the lithosphere younger than 1 Ma. If the apparent absence of the gravity lineaments near the ridge axis (Figure 1b) is interpreted as indicating a fracture resistance of the lithosphere to the developing thermoelastic stress, our modeling results may be used to put an upped bound on the effective fracture energy of the lithosphere. For the parameters used in Figure 9, the corresponding energy is of the order of $QL/H \sim 10^7$-10^8 Jm^{-2}.

Our simple model explains both the wavelength and amplitude of the gravity lineaments observed on young seafloor (Figure 5). The solid curves in Figure 5 are the band-pass filtered gravity profiles at 8 ages. The more regular grey curves are the predictions of the model using an onset age corresponding to the present seafloor age. These were computed by assuming uncompensated seafloor topography with uniform crustal thickness (ρ_c=2800 kg m^{-3}; ρ_m=3300 kg m^{-3}; 6 km crustal thickness). The model gravity profiles were low-pass filtered at 80-km wavelength to match the processing of the observed profiles and they were also scaled by 0.75 to provide a better visual match. This reduced amplitude may reflect incomplete cracking of the plate or an overestimate of Young's modulus used in the model calculation. Note the excellent agreement in amplitude and wavelength at ages of 0.5, 3.2, 5.7, and 8.2 Ma. At greater ages the model slightly overpredicts both the amplitude and the wavelength of the anomalies. Of course, for the real oceanic lithosphere that ages continuously away from the ridge axis, there is a third dimension that we have not considered.

Conclusions

Our improved gravity model derived from the ERS satellite altimeter data allows us to robustly resolve both the gravity lineaments and volcanic ridges on the central Pacific seafloor, as confirmed by comparisons with more limited shipboard surveys. We find that volcanic ridges preferentially occur in the troughs of the gravity lineaments. Modeling of the effects of the volcano-induced flexure on the gravity field demonstrates that the gravity lows cannot be explained by the volcanic loads, which essentially rules out a convective origin of the observed gravity lineaments. The satellite altimetry data indicate that lineaments are absent at the EPR axis but develop rapidly on young seafloor on both sides of the spreading ridge. On the Pacific plate they cross the grain of the older seafloor spreading fabric, suggesting that the gravity lineaments manifest an on-going tectonic process. We develop a model for thermoelastic flexure of a cracked plate using well-constrained parameters of the plate cooling model and the yield strength envelope model. Elastic energy released by thermoelastic flexure has a pronounced maximum at a crack spacing of 3.4 times the flexural parameter of the cooling plate. Our model matches both the wavelength and amplitude of the observed gravity lineaments. The thermoelastic cracking provides conduits for the escape of available magma to the surface resulting in volcanic ridge formation. The cracks are predicted to align perpendicular to the least compressive stress within the plate. The apparent obliqueness of the gravity lineaments to the older seafloor fabric implies a change in the stress orientation since the old fabric formation. This uniform orientation of the gravity lineaments combined with their increasing wavelength with increasing seafloor age, suggest they were initiated sometime during the past 5-7 Ma and their development continues today. Because the thermoelastic deformation is an intrinsic feature of the plate spreading, our model predicts that the seafloor corrugations and volcanic ridges should be ubiquitous features of the ocean basins. However, the more closely spaced transform faults on the slow spreading ridges may prevent the development of significant thermoelastic stress. Moreover, because the flexures have low amplitude (~200 m) they will only observable on the flanks of the fastest spreading ridges where the sediment cover is minimal, and the ambient topography is smooth.

Acknowledgements: Correspondence and requests for materials should be addressed to David T. Sandwell. (e-mail: dsandwell@ucsd.edu. This work was supported by NSF OCE03-26707 and NASA NAG5-13673.

References

Abers, G.A., B. Parsons, and J.K. Weissel, Seamount abundances and distributions in the southeast Pacific, *Earth Planet. Sci. Lett.*, *87*, 137-151, 1988.

Atkinson, B.K., *Fracture Mechanics of Rock*, pp 1-23 pp., Academic Press, London, 1987.

Bergman, E.A., and S.C. Solomon, Source mechanisms of earthquakes near mid-ocean ridges from body waveform inversion, implications for the early evolution of oceanic lithosphere, *J. Geophys. Res.*, *89*, 11415-11444, 1984.

Boley, B., and J.H. Weiner, *Theory of Thermal Stress*, 586 pp. pp., John Wiley & Sons, Inc., New York, 1960.

Bratt, S.R., E.A. Bergman, and S.C. Solomon, Thermoelastic stress: How important as a cause of earthquakes in young lithosphere?, *J. Geophys. Res.*, *90*, 10249-10260, 1985.

Buck, W.R., and E.M. Parmentier, Convection beneath young oceanic lithosphere: Implications for thermal structure and gravity, *J. Geophys. Res.*, *91*, 1961-1974, 1986.

Dunbar, J., and D.T. Sandwell, A boudinage model for crossgrain lineations, *Eos Trans. AGU*, *69*, 1429, 1988.

Fialko, Y.A., On origin of near-axis volcanism and faulting at fast spreading mid-ocean ridges, *Earth. Planet. Sci. Lett.*, *190*, 31-39, 2001.

Fialko, Y.A., and A.M. Rubin, Numerical simulation of high pressure rock tensile fracture experiments: Evidence of an increase in fracture energy with pressure?, *J. Geophys. Res.*, *102*, 5231-5242, 1997.

Fleitout, L., C. Dalloubeix, and C. Moriceau, Small-wavelength geoid and topography anomalies in the South Atlantic Ocean - a clue to new hot-spot tracks and lithospheric deformation, *Geophys. Res. Lett.*, *16* (7), 637-640, 1989.

Forsyth, D., S. Webb, D. Scheirer, C. Langmuir, R. Duncan, and K. Donnelly, COOK16MV Cruise Report R/V Melville; tahiti - Easter I., 8 November - 24 November, 2001, pp. 20 pp, Brown Univ., Providence RI, 2002.

Gans, K.D., D.S. Wilson, and K.C. Macdonald, Pacific plate gravity lineaments: Extension or thermal contraction?, *Geochemistry, Geophysics, Geosystems*, *in press*, 2003.

Goetze, C., and B. Evans, Stress and temperature in the bending lithosphere as constrained by experimental rock mechanics, *Geophys. J. R. astr. Soc.*, *59*, 463-478, 1979.

Goodwillie, A.M., and B. Parsons, Placing bounds on lithospheric deformation in the central Pacific Ocean, *Earth Planet. Sci. Lett.*, *111*, 123-139, 1992.

Goodwillie, A.M., and A.B. Watts, An altemitric and bathymetric study of elastic thickness in the central Pacific Ocean,, *Earth Planet. Sci. Lett.*, *118*, 311-326, 1993.

Haxby, W.F., and J.K. Weissel, Evidence for small-scale mantle convection from Seasat altimeter data, *J. Geophys. Res.*, *91* (B3), 3507-3520, 1986.

Husseini, M.I., Energy balance for formation along a fault, *Geophys. J. R. astr. Soc.*, *49*, 699-714, 1977.

Janney, P.E., J.D. Macdougall, J.H. Natland, and M.A. Lynch, Geochemical evidence from Pukapuka volcanic ridge system for a shallow enriched mantle domain beneath the South Pacific Superswell, *Earth. Planet. Sci. Lett.*, *181*, 47-60, 2000.

Lynch, M.A., Linear ridge groups: Evidence for tensional cracking in the Pacific Plate, *J. Geophys. Res.*, *104* (B12), 29321-29333, 1999.

Maus, S., C.M. Green, and J.D. Fairhead, Improved ocean-geoid resolution from retracked ERS-1 satellite altimeter waveforms, *Geophys. J. Int.*, *134* (N1), 243-253, 1998.

Morgan, W.J., Convection plumes in the lower mantle, *Nature*, *230*, 42-43, 1971.

Parmentier, E.M., and W.F. Haxby, Thermal stress in the oceanic lithosphere: Evidence from geoid anomalies at fracture zones, *J. Geophys. Res.*, *91*, 7193-7204, 1986.

Parsons, B., and J.G. Sclater, An analysis of the variation of the ocean floor bathymetry and heat flow with age, *J. Geophys. Res.*, *82*, 803-827, 1977.

Parsons, T., and G.A. Thompson, The role of magma overpressure in suppressing earthquakes and topography: Worldwide examples, *Science*, *253*, 1300-1302, 1991.

Ricard , Y., and C. Froidevaux, Stretching instabilities and lithospheric boudinage, *J. Geophys. Res.*, *91*, 8314-8324, 1986.

Richter, F.M., and B. Parsons, On the interaction of two scales of convection in the mantle, *J. Geophys. Res.*, *80*, 2529-2541, 1975.

Sandwell, D.T., Thermal Stress and the Spacings of Transform Faults, *J. Geophys. Res.*, *91* (B6), 6405-6417, 1986.

Sandwell, D.T., and W.H.F. Smith, Marine gravity anomaly from Geosat and ERS-1 satellite altimetry, *J. Geophys. Res.*, *102* (B5), 10039-10054, 1997.

Sandwell, D.T., E.L. Winterer, J. Mammericks, R.A. Duncan, M.A. Lynch, D.A. Levitt, and C.L. Johnson, Evidence for diffuse extension of the Pacific Plate from Puka-puka ridges and Cross-grain gravity lineations, *J. Geophys. Res.*, *100*, 15087-15099, 1995.

Scholz, C.H., *The mechanics of earthquakes and faulting*, 496 pp. pp., Cambidge Univ. Press, New York, 2002.

Searle, R.C., J. Francheteau, and B. Cornaglia, New Observations on mid-plate volcanism and the tectonic history of the Pacific plate, Tahiti to Easter Microplate, *Earth. Planet. Scis. Lett.*, *131*, 395-421, 1995.

Shen, Y., D.W. Forsyth, J. Conder, and L.M. Dorman, Investigation of microearthquake activity following an intraplate teleseismic swarm on the flank of the southern East Pacific Rise, *J. Geophys. Res.*, *102*, 459-475, 1997.

Sleep, N.H., Hotspot volcanism and mantle plumes, *Ann. Rev. Earth Planet. Sci.*, *20*, 19-43, 1992.

Turcotte, D.L., Are Transform Faults Thermal Contraction Cracks?, *J. Geophys. Res.*, *79*, 2573-2577, 1974.

Weins, D.A., and S. Stein, Intraplate seismicity and stress in young oceanic lithosphere, *J. Geophys. Res.*, *89*, 11442-11464, 1984.

Wessel, P., Thermal stress and the bimodal distribution of elastic thickness estimates of the oceanic lithosphere, *97*, 14177-14193, 1992.

Winterer, E.L., and D.T. Sandwell, Evidence from en-echelon cross-grain ridges for tensional cracks in the Pacific Plate, *Nature*, *329* (6139), 534-537, 1987.

Woo, T.C., Thermal stress problems in glass, *J. Applied Physics*, *39* (4), 2082-2087, 1968.

Figures

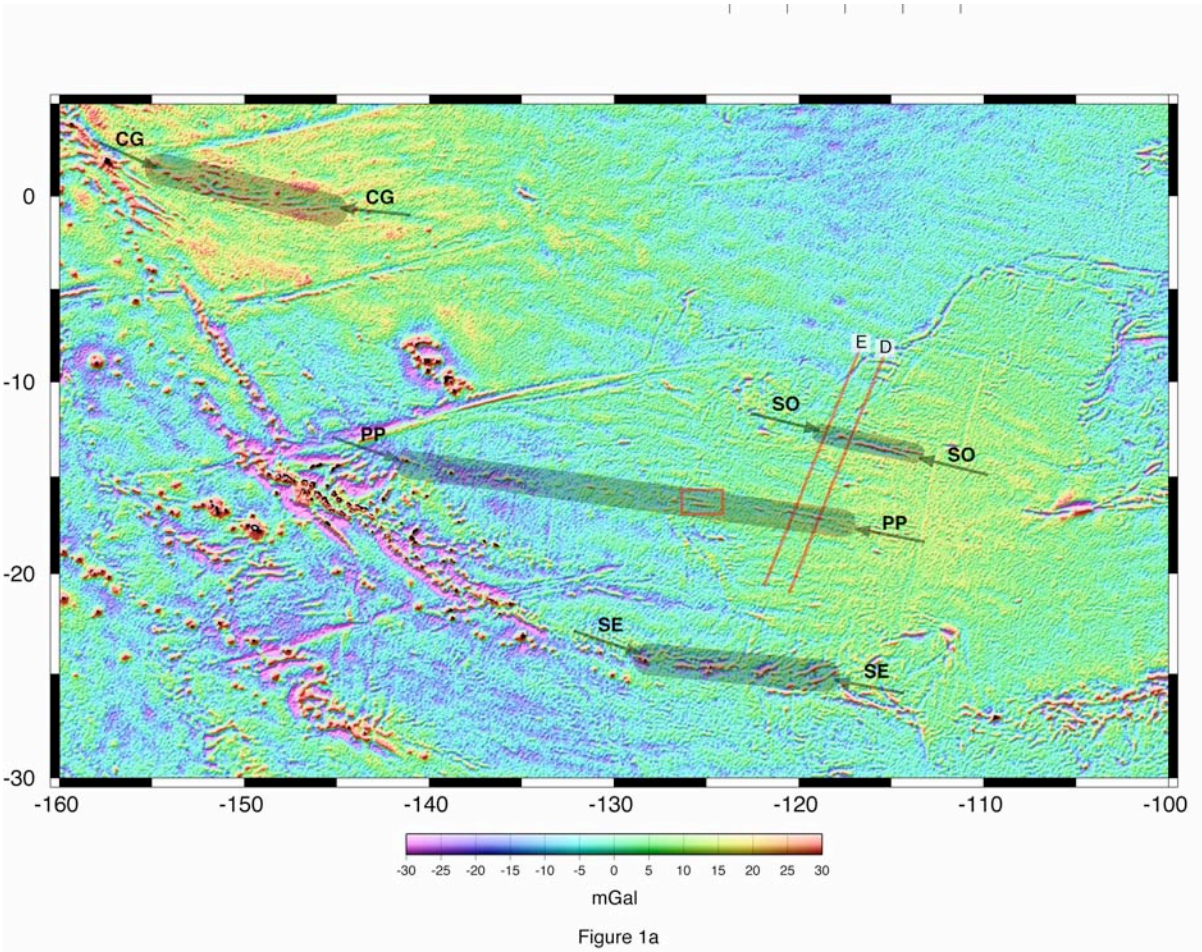

Figure 1. (a) Gravity anomaly derived from re-tracked ERS-1 radar altimeter data, Geosat altimeter data, and Topex altimeter data provides improved accuracy and resolution to reveal the close association between the gravity lineaments and the volcanic ridges. Red lines are tracklines of R/V Conrad where bathymetry and gravity profiles were collected (see Figure 4). Red box outlines a part of the Pukapuka ridges that was surveyed by R/V Melville (see Figure 2) [*Sandwell et al.*, 1995]. Prominent volcanic ridges in the area include Crossgrain ridges [*Winterer and Sandwell*, 1987] CG; Pukapuka ridges [*Sandwell et al.*, 1995] PP; the ridges of *Searle et al.* [1995] SE; and most recently the Sojourn Ridges [*Forsyth et al.*, 2002] SO.

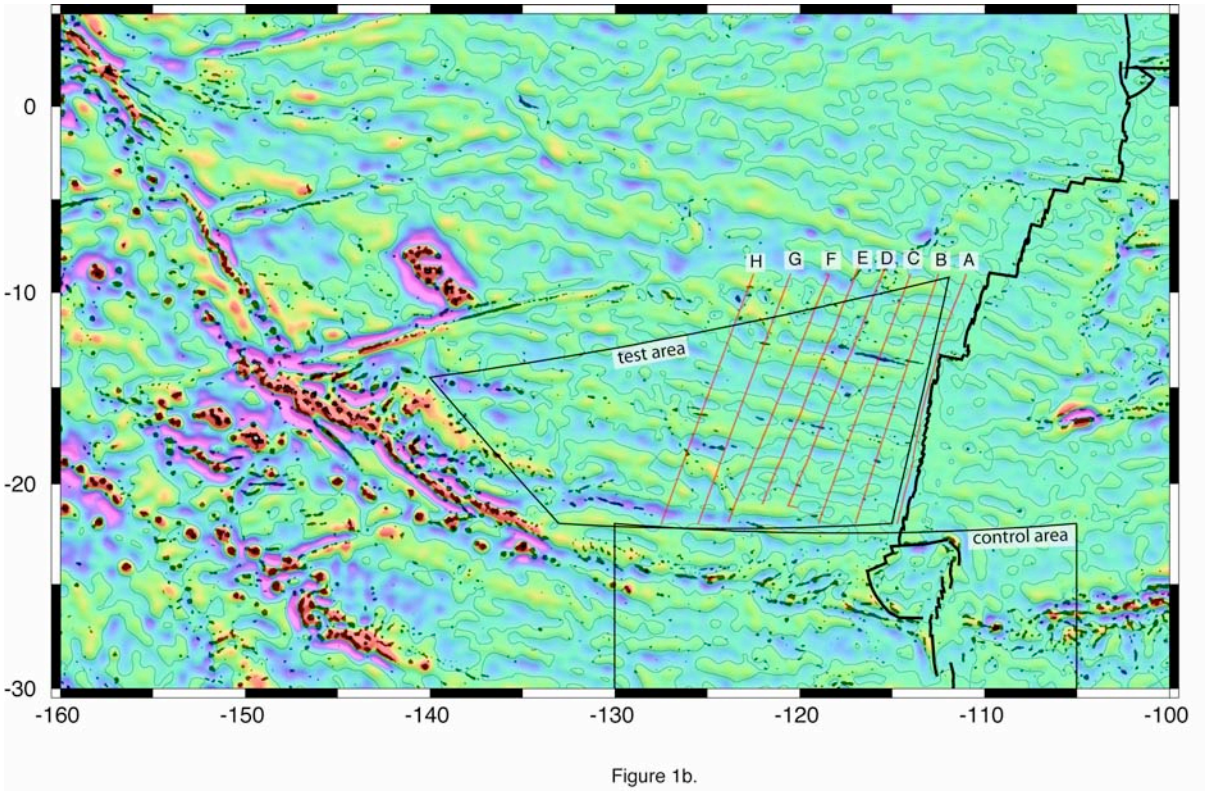

Figure 1 (b) Band-pass filtered gravity anomaly ($80 < l < 600$ km) derived from re-tracked satellite altimeter data. Color scale saturates at $\pm$15 mGal. Gravity lineaments with 140-km wavelength develop between the ridge axis and 6 Ma. Lineaments on older seafloor have somewhat longer wavelength (~180 km) and cross the grain of the seafloor spreading fabric. Gravity lineaments also occur on the Nazca plate to the east of the East Pacific Rise. Seamounts and volcanic ridges are marked as black areas. Many of these volcanic chains are geometrically associated with the gravity lineaments. The morphology of three sets of these ridges indicates that they formed by N-S tension of the Pacific plate [*Lynch*, 1999]. The longest of these ridge groups, the Pukpuka ridges, extends for over 2600 km from 5 Ma old seafloor near the East Pacific Rise to 45 Ma old seafloor near the Tuamotu Archipelago.

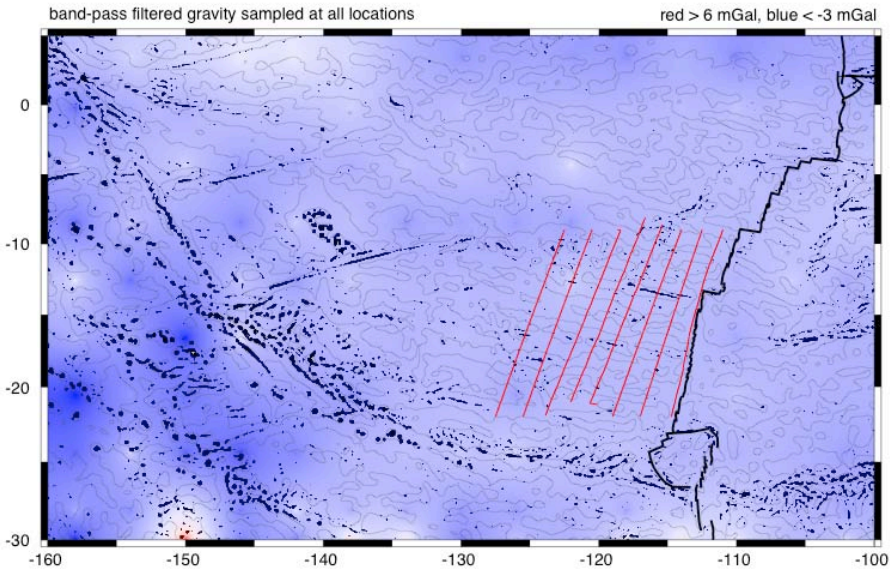

Figure 1c.

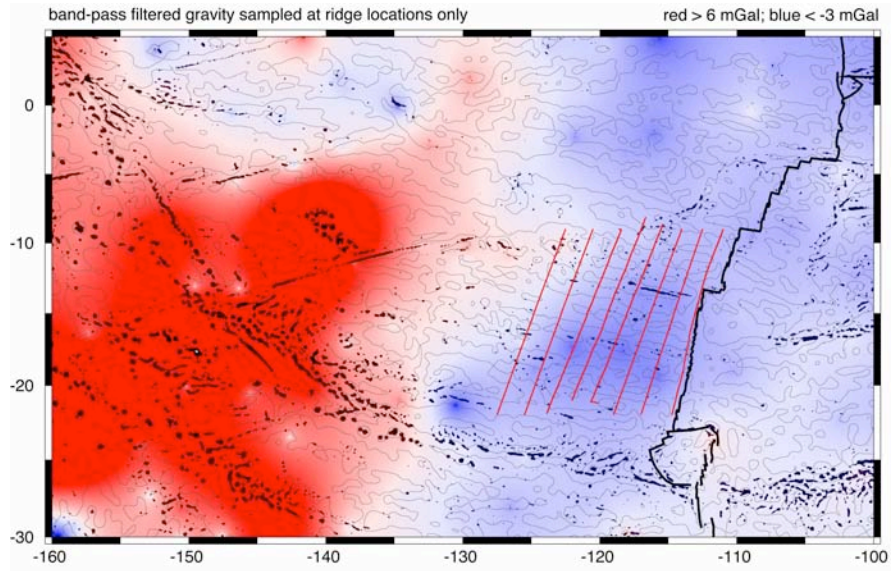

Figure 1d.

Figure 1 (c) Band-pass filtered gravity anomaly ($80 < l < 600$ km) sampled at all locations and and median filtered over a diameter of 450 km (red > 6 mGal; blue < -3 mGal). Because the band-pass filtered data are evenly sampled they have nearly zero mean and median everywhere. (Perhaps this is a useless figure but it further emphasizes that finding predominately negative band-pass filtered gravity at volcanic ridges is highly anomalous.)

Figure 1 (d) Band-pass filtered gravity anomaly ($80 < l < 600$ km) sampled at locations of volcanic ridges and seamounts and median filtered over a diameter of 450 km (red > 6 mGal; blue < -3 mGal). Airy and flexural compensation models predict the band-pass filtered gravity should be > 1.5 mGal at volcanic loads. Areas of pronounced gravity lineaments have negative band-pass filtered gravity at volcanic ridges.

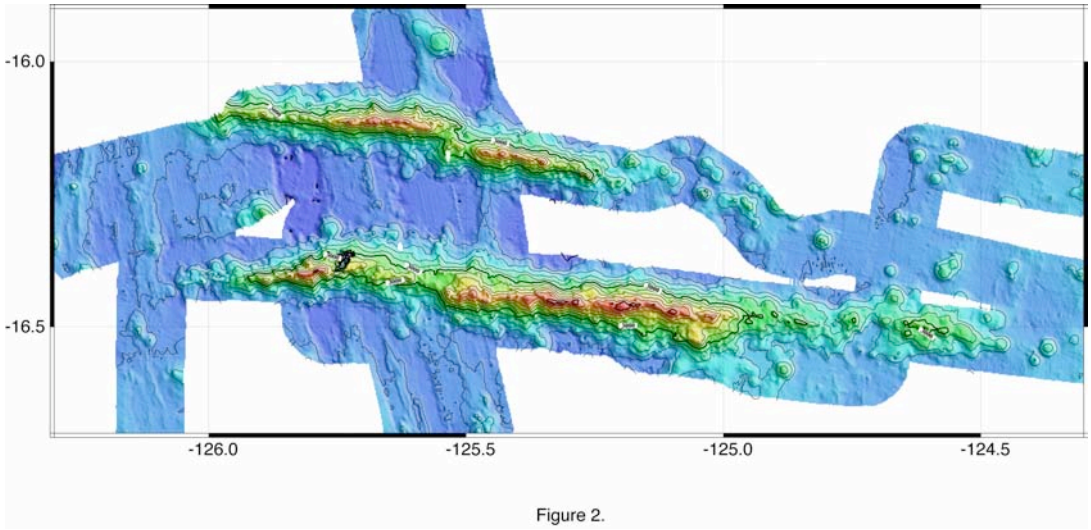

Figure 2.

Figure 2. Detailed bathymetry (200-m contour interval) of a pair of volcanic ridges along the Pukapuka chain [*Sandwell et al.*, 1995]. The ridges are about 2 km tall, 10 km wide and 75/150 km long. These ridges formed 9 Ma ago and are on seafloor that is 19 Ma. Notice that the ridges are not perpendicular to the abyssal hill fabric.

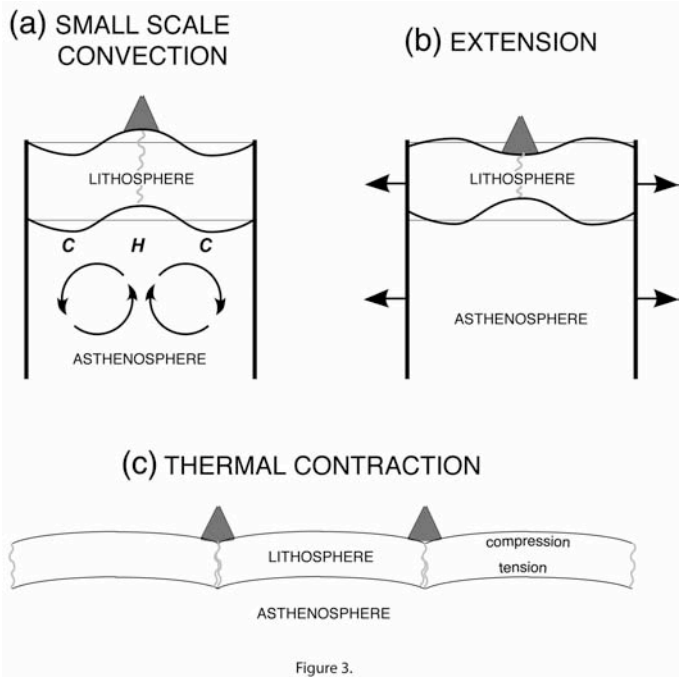

Figure 3.

Figure 3. Models for the formation of the gravity lineaments and en-echelon volcanic ridges. (a) Small-scale convection cells develop beneath cooled lithosphere and align in the direction of absolute plate motion by shear in the asthenosphere [*Richter and Parsons*, 1975; *Buck and Parmentier*, 1986]. Volcanoes develop above the hot upwelling axis of the cell. (b) Slow and diffuse extension creates lithospheric boudinage structures [*Ricard and Froidevaux*, 1986]. Volcanoes develop in the troughs (maximum strain) if partially melted mantle is available beneath the plate [*Sandwell et al.*, 1995]. (c) Thermoelastic flexure will develop if the lithosphere is cracked at a regular intervals [*Gans et al.*, 2003]. Volcanoes will develop above the cracks if partially melted mantle is available beneath the plate.

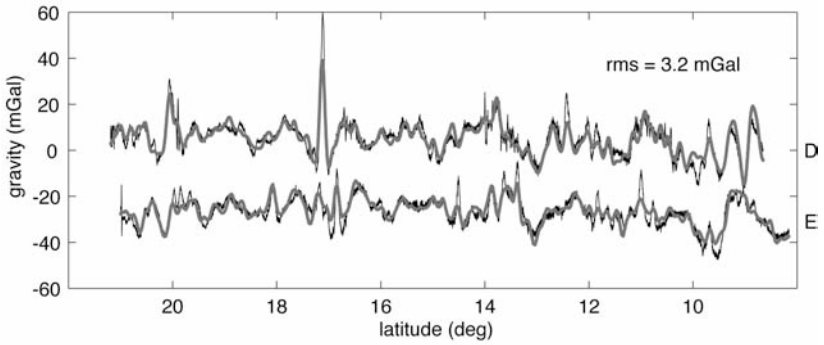

Figure 4.

Figure 4. Comparison between shipboard (black) and satellite-derived (grey) gravity anomalies along profiles D and E (Figure 1) [*Abers et al.*, 1988] has 3.2 mGal rms deviation. The improved resolution and accuracy of the re-tracked ERS-1 altimeter data is used to better delineate the volcanic ridges.

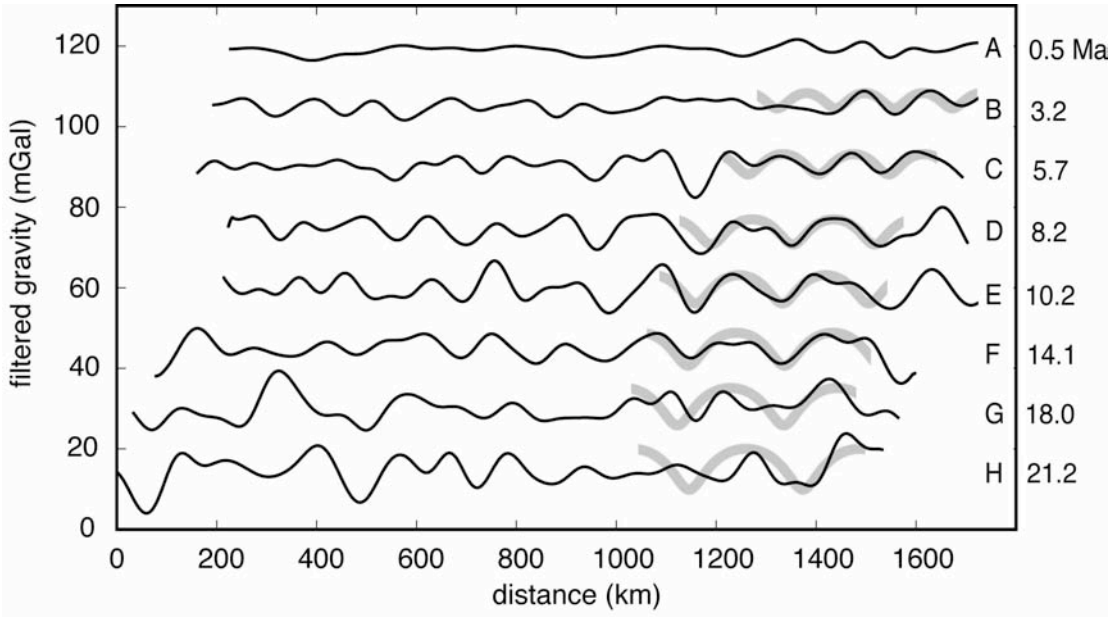

Figure 5.

Figure 5. Ship [*Abers et al.*, 1988] and satellite-derived gravity profiles parallel to the east Pacific Rise crest reveal the development of the gravity lineaments. 2-D filtering of the satellite-derived gravity reveals the development of the seafloor undulations. Undulations are not apparent at the ridge axis (profile A) but develop rapidly on 3.2 Ma seafloor (Profile B) and are fully developed on 7-12 Ma seafloor. Model predictions (grey lines) match the amplitude and wavelength of the observed seafloor undulations between 0 and 12 Ma. The model over-predicts both the amplitude and wavelength of gravity lineaments on older seafloor (> 14 Ma).

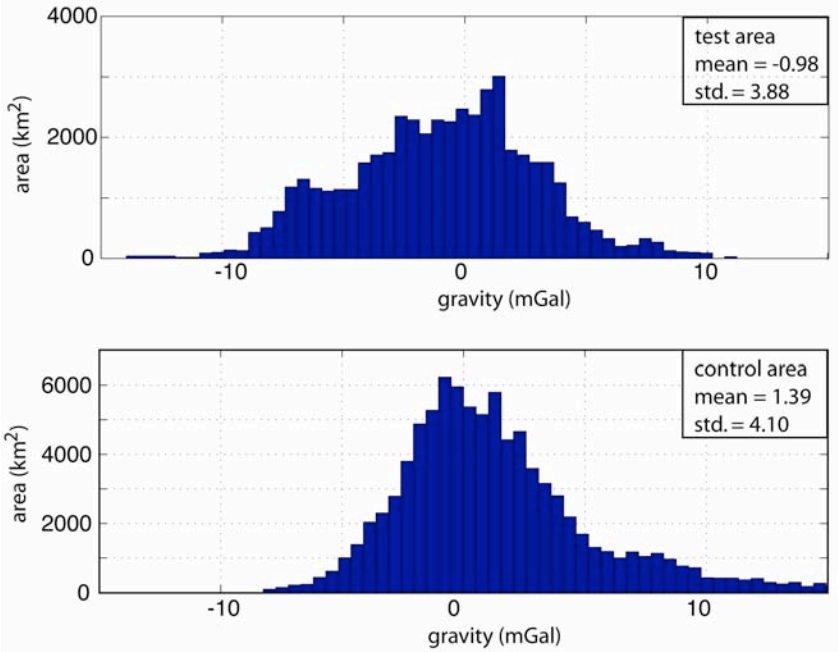

Figure 6.

Figure 6. Histograms of the area of volcanic ridge seafloor versus band-pass filtered gravity. (upper) The histogram of the test area covered by prominent volcanoes (see Figure 1) has a mean of –0.98, a median of –0.73, and a standard deviation of 3.88. (lower) The histogram of the portion of the control area covered by prominent volcanoes has a mean of 1.39, a median of 0.70, and a standard deviation of 4.10. This difference in mean gravity between the test area and the control area (-2.38 mGal) is consistent with the hypothesis that volcanic ridges in the test area preferentially occur in the troughs of the gravity anomalies.

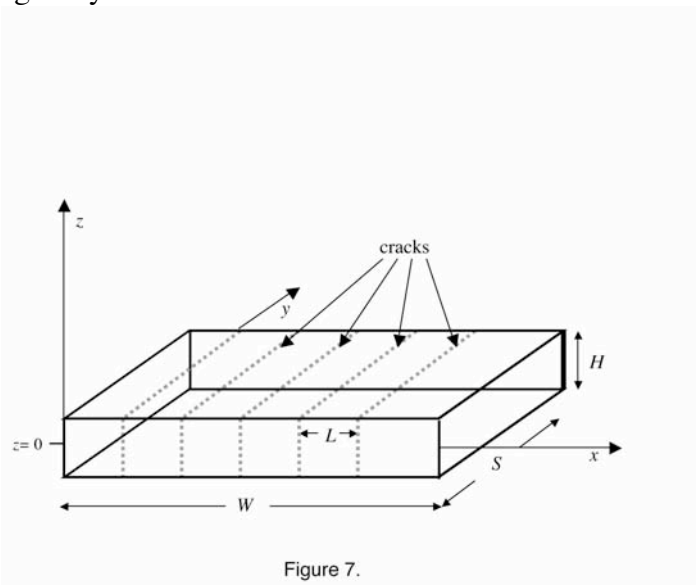

Figure 7.

Figure 7. Thin elastic plate of thickness H, length S, and width W, contains N cracks with spacing of L.

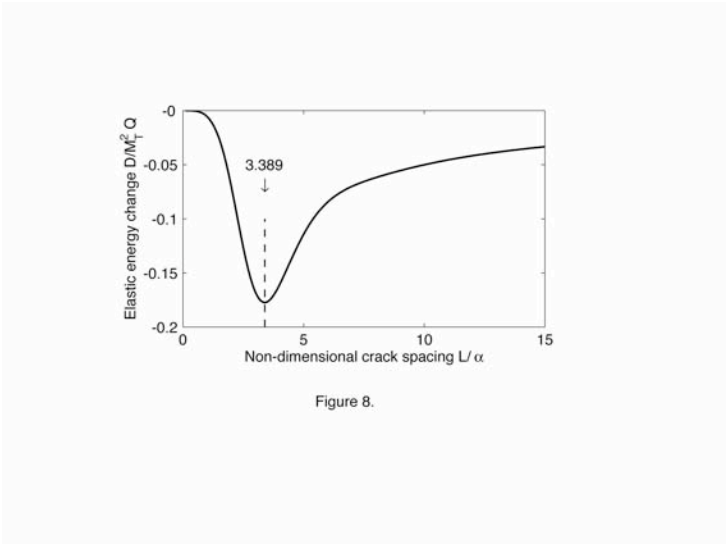

Figure 8. Model prediction for the thermoelastic energy release as a function non-dimensional crack spacing L/α. Minimum in the potential energy of elastic deformation of the plate occurs when $L = 3.389\ \alpha$.

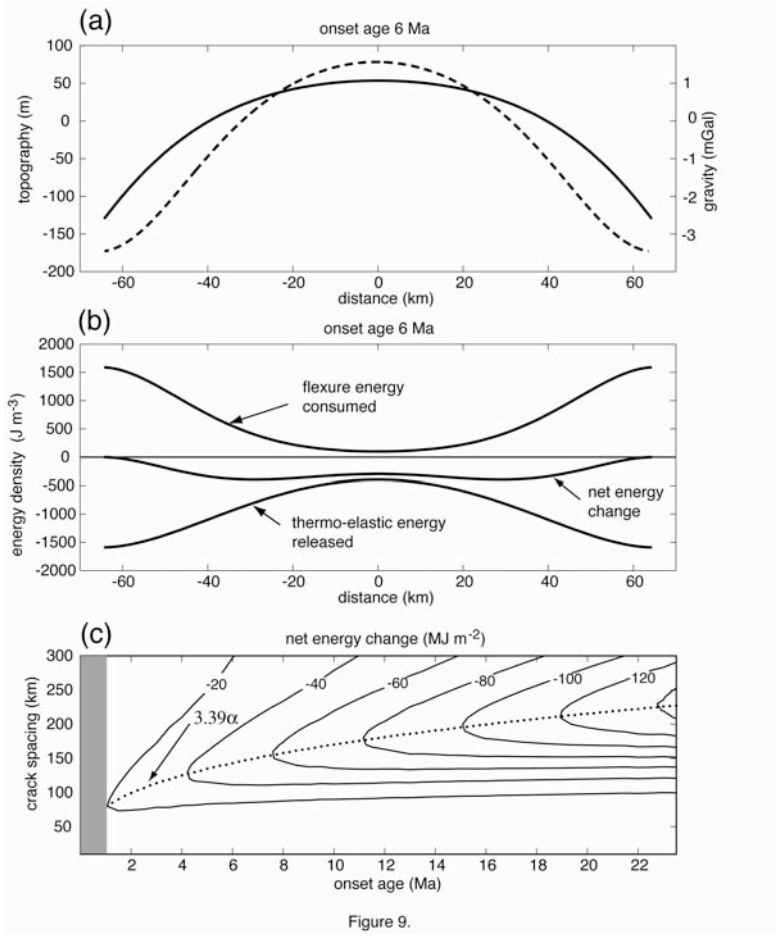

Figure 9. (a) Model of thermoelastic flexure where 130-km spaced cracks are introduced at 6 Ma (solid curve – 230 m amplitude topography, dashed curve – 5 mGal amplitude gravity anomaly). (b) Thermoelastic energy released by concave down bending exceeds energy consumed by flexing the plate. (c) Net energy versus crack spacing and crack onset age shows a minimum at 3.39 times the flexural parameter α.